Accepted by ApJ
Preprint typeset using LaTeX style emulateapj v. 03/07/07

arXiv:1512.02633v1 [astro-ph.GA] 8 Dec 2015

EXPLORING X-RAY BINARY POPULATIONS IN COMPACT GROUP GALAXIES WITH CHANDRA

P. Tzanavaris[1,2,3], A. E. Hornschemeier[1], S. C. Gallagher[4], L. Lenkić[4], T. D. Desjardins[5], L. M. Walker[6], K. E. Johnson[7], J. S. Mulchaey[8]

Accepted by ApJ

ABSTRACT

We obtain total galaxy X-ray luminosities, L_X, originating from individually detected point sources in a sample of 47 galaxies in 15 compact groups of galaxies (CGs). For the great majority of our galaxies, we find that the detected point sources most likely are local to their associated galaxy, and are thus extragalactic X-ray binaries (XRBs) or nuclear active galactic nuclei (AGNs). For spiral and irregular galaxies, we find that, after accounting for AGNs and nuclear sources, most CG galaxies are either within the $\pm1\sigma$ scatter of the Mineo et al. (2012) L_X - star formation rate (SFR) correlation or have higher L_X than predicted by this correlation for their SFR. We discuss how these "excesses" may be due to low metallicities and high interaction levels. For elliptical and S0 galaxies, after accounting for AGNs and nuclear sources, most CG galaxies are consistent with the Boroson et al. (2011) L_X - stellar mass correlation for low-mass XRBs, with larger scatter, likely due to residual effects such as AGN activity or hot gas. Assuming non-nuclear sources are low- or high-mass XRBs, we use appropriate XRB luminosity functions to estimate the probability that stochastic effects can lead to such extreme L_X values. We find that, although stochastic effects do not in general appear to be important, for some galaxies there is a significant probability that high L_X values can be observed due to strong XRB variability.

Subject headings: X-rays: galaxies – X-rays: binaries

1. INTRODUCTION

Most galaxies in the local Universe are found within poor groups (Mulchaey 2000 and references therein; Karachentsev et al. 2005). Studying the physical processes in these systems is thus fundamental to understanding galaxy formation and evolution, which remains one of the key goals of extragalactic astrophysics.

Compact galaxy groups constitute an extreme class of such small galaxy systems. The separations of galaxies in these systems are typically of the order of just a few galaxy radii, with median projected separations $\sim 40h^{-1}$ kpc[9]); velocity dispersions are low, with a radial median $\sim$ 200 km s^{-1}, while galaxy number densities are high (up to 10^8h^2 Mpc^{-2}, Hickson 1982; Hickson et al. 1992). Thus CGs are environments where galaxy interactions are prevalent. Such interactions give rise to tidal tails and favor collapse of giant molecular clouds, thus affecting star formation and its evolution (e.g. Mihos & Hernquist 1996).

Star formation in CG galaxies appears to be accelerated when compared to galaxies that do not reside in such an environment. This in turn likely leads to fast consumption of the available gas and abrupt quenching. The observational signatures of this are "gaps" both in mid-infrared colors (Johnson et al. 2007; Walker et al. 2010, 2012) as well as mass-normalized star formation rates (specific SFRs, sSFRs, Tzanavaris et al. 2010, Lenkic et al. 2015, in prep.). The latter works further suggest that the more strongly star-forming galaxies are preferentially hosted by CGs which are richer in H I gas, and vice versa for galaxies that show low levels of star-forming activity.

The interaction-prone CG environment may also affect the type and level of activity occurring in the *nuclei* of CG galaxies. For instance, simulations have shown that major and minor galaxy mergers can often bring about inflow of rotationally supported gas from the outer parts of a galaxy to fuel central supermassive black hole activity via accretion ("AGNs", e.g. Hopkins & Quataert 2010), and this is corroborated by observations (e.g. Kartaltepe et al. 2010). Several works using a variety of multi-wavelength data and methods have shown that, although CGs do host substantial *numbers* of AGNs, the *level* of this activity does not, in general, appear to be high (see Tzanavaris et al. 2014, hereafter T14, and references therein).

X-ray emission provides an alternative path to probing star formation in the CG environment. Broadly speaking, for galaxies without strong X-ray AGNs, X-ray emission is dominated by X-ray binary stars (XRBs), where a compact primary, either a neutron star or black hole, accretes matter from either a low-mass (LMXBs) or a high-mass (HMXBs) donor secondary in early- and late-type galaxies, respectively (Kim et al. 1992). Thanks to the *Chandra* X-ray telescope's sub-arcsecond resolution, it is now possible to detect such individual X-ray point

[1] Laboratory for X-ray Astrophysics, NASA/Goddard Space-flight Center, Mail Code 662, Greenbelt, Maryland, 20771, USA
[2] CRESST, University of Maryland Baltimore County, 1000 Hill-top Circle, Baltimore, MD 21250, USA
[3] Department of Physics and Astronomy, The Johns Hopkins University, Baltimore, MD 21218, USA
[4] Department of Physics and Astronomy & Centre for Planetary and Space Exploration, The University of Western Ontario, Lon-don, ON N6A 3K7, Canada
[5] Department of Physics and Astronomy, 177 Chem.-Phys. Building, University of Kentucky, 505 Rose Street, Lexington KY 40506-0055202, USA
[6] Steward Observatory, University of Arizona, Tucson, AZ 85721, USA
[7] Department of Astronomy, University of Virginia, P.O. Box 400325, Charlottesville, VA 22904-4325, USA
[8] The Observatories of the Carnegie Institution for Science, Pasadena, CA 91101, USA
[9] $h \equiv H_0/100$, where H_0 is the Hubble constant at redshift 0.

sources in nearby galaxies (see, e.g. Fabbiano 2006, and references therein). If these sources are offset from a galaxy's nucleus, these are most likely either LMXBs or HMXBs. Combined with the estimated high binarity fraction in stellar populations, the study of these sources can provide key information for galaxies as a whole. The situation is less clear for nuclear sources because their X-ray emission may come from an AGN, star formation (e.g. Rossa et al. 2006), or both types of activity.

In actively star-forming (morphologically spiral/irregular) galaxies, the SFR is traced by populations of massive, luminous, and short lived ($\lesssim$ 100 Myr) OB associations. Some of these stars will be HMXB secondaries: Indeed several studies of late-type galaxies have established strong correlations between galaxy-wide X-ray luminosity and total SFR (e.g. Bauer et al. 2002; Grimm et al. 2003; Ranalli et al. 2003; Gilfanov et al. 2004a; Persic et al. 2004; Hornschemeier et al. 2005; Persic & Rephaeli 2007; Lehmer et al. 2008, 2010; Mineo et al. 2012). On the other hand, in quiescent (morphologically elliptical/S0) galaxies, longer-lived ($\gtrsim$ 1 Gyr) low-mass stars trace the total stellar mass accumulated over a galaxy's lifetime. Such stars may be LMXB donors, which explains the observed correlations between an early-type galaxy's X-ray luminosity and total stellar mass, M_* (e.g. Fabbiano & Shapley 2002; Gilfanov 2004; Kim et al. 2004; Lehmer et al. 2010; Boroson et al. 2011).

Clearly, this is an oversimplified picture. Many galaxies will have a mix of HMXB and LMXB populations, such as ellipticals with residual star formation or bulge-dominated spirals. In general detailed modeling is therefore required to understand the contributions of different sub-populations to the total X-ray point-source luminosity both for late- and for early-type galaxies (see Luo et al. 2012, for a population synthesis based analysis of a combined LMXB and HMXB population).

Mineo et al. (2012, hereafter M12) study 29 nearby ($<$ 20 Mpc) galaxies[10]. This "primary" sample is selected based on several criteria, such as morphologies, sSFR threshold, identification and exclusion of bulge sources, and sensitivity to ensure that their systems are late-types dominated by resolved HMXB emission. They also perform detailed corrections for incompleteness at the low luminosity end. The galaxies in this primary sample (up to $\lesssim 20\ M_{\odot}\mathrm{yr}^{-1}$) include the moderate SFR range, which is representative of CG galaxies, and have a variety of late-type morphologies, providing a control sample for CG late-type systems.

In their study of 17 nearby ($<$ 60 Mpc) luminous IR galaxies, Lehmer et al. (2010) take advantage both of high-resolution imaging with *Chandra* and spectral information to disentangle the contributions of AGNs, XRBs and hot gas. They parameterize and obtain best fits for the combined contributions of LMXBs and HMXBs as functions of M_* and SFR, respectively. Their sample was selected by proximity and low column density, in order to maximize separability of the various contributions to X-ray emission. Lehmer et al. (2010) perform fits as functions of sSFR; however their sSFR regime does not cover the substantial low-sSFR CG regime. A direct comparison of CGs with these fits may then be not particularly useful.

Boroson et al. (2011, hereafter B11) study exclusively X-ray emission from 30 early-type galaxies observed with *Chandra* to a depth that allows the detection of individual LMXBs with $L_X > 10^{38}$ erg s^{-1}. In their analysis, they estimate in detail the separate contributions to the total X-ray luminosity due to active binaries (ABs), cataclysmic variables (CVs), hot gas and LMXBs. They thus obtain a scaling relation between $L_{X,\mathrm{LMXB}}$ and K-band luminosity, L_K, which traces old stellar populations and, hence, stellar mass.

The B11 sample is well-matched in stellar mass to the CG sample and is thus suitable as a comparison sample for the LMXB emission from CG early-type galaxies.

We have already studied *diffuse* X-ray emission in CGs in two recent publications. In Desjardins et al. (2013) and Desjardins et al. (2014) we detect diffuse X-ray emission in a majority of CGs. In dynamically unevolved systems, characterized by low masses and velocity dispersions, we find that this emission originates in processes local to the galaxies (star formation, AGNs or tidal tails) and appears directly linked to individual galaxies rather than a diffuse intragroup medium (IGM).

In this paper we use *Chandra* archival data to detect individual X-ray point sources in a sample of 47 CG galaxies. The aim of the paper is to assess whether, and to what extent, point-source based galaxy luminosities for CG galaxies agree with the L_X - SFR and L_X - M_* correlations for late- and early-type galaxies, respectively. The structure of the paper is as follows: Section 2 describes the CG data sample. Section 3 discusses X-ray data and analysis, with emphasis on point source and galaxy-wide luminosities, as well as stochastic effects, and local and background AGN contamination. Section 4 is a brief description of the SFR and M_* obtained via non-X-ray work, which is presented in a separate forthcoming publication (Lenkic et al. 2015, L15, in prep.). Section 5 presents our CG results within the context of X-ray luminosity scaling relations. We discuss these results in Section 6, and summarize in Section 7. We use $\Omega_M = 0.3$, $\Omega_\Lambda = 0.7$, and $H_0 = 70$ km s^{-1}Mpc^{-1} throughout.

2. SAMPLE SELECTION

In this paper we study a sample of 15 compact groups observed with *Chandra*/ACIS, *Swift*/UVOT and *Spitzer*/IRAC-MIPS for which archival data exist, allowing us to obtain SFRs, stellar masses, sSFRs and X-ray fluxes and luminosities. Table 1 shows the group sample, including redshifts, luminosity distances and group evolutionary types. Allowing for the fact that some galaxies do not fall in the field of view of all three instruments, the total number of CG galaxies analyzed is 47.

The majority of the CGs analyzed here are from the catalog of 92 CGs that have been spectroscopically confirmed by Hickson et al. (1992). As in Tzanavaris et al. (2010) and Tzanavaris et al. (2014) the selection criteria for this sample aimed to allow observations with a range of telescopes and instruments, both space and ground-based. We thus demanded that a CG contain at least three giant galaxies with "accordant" redshifts within 1000 km s^{-1} of the group's mean redshift, be closer than $\sim$ 4500 km s^{-1}, and span less than $\sim 8'$ on the sky. In spite of concerns about selection biases in the

[10] With the exception of one galaxy at $\sim$ 123 Mpc.

TABLE 1
Compact Group Sample

ID	z	v (km s^{-1})	D_L (Mpc)	H I type	*Chandra* X-ray obs. IDs	ACIS	ks	refs
(1)	(2)	(3)	(4)	(5)	(6)	(7)	(8)	(9)
HCG 7	0.0141	3885	56.0	II	8171, 9588	S	36.3	T14
HCG 16	0.0132	3706	53.4	II	923	S	12.7	T14
HCG 22	0.0090	2522	36.3	II	8172	S	32.2	T14
HCG 31	0.0135	4026	58.1	I	9405	S	36.0	T14
HCG 37	0.0223	6940	101.0	III	5789	S	17.9	D14
HCG 40	0.0223	7026	102.0	II	5788, 6203	S	48.3	D14
HCG 42	0.0133	4332	62.6	II	3215	S	32.1	T14
HCG 59	0.0135	4392	63.5	III	9406	S	38.9	T14
HCG 62	0.0137	4443	68.7	III	921, 10462, 10874	S	169.2	T14
HCG 79	0.0145	4439	64.1	II	11261	S	69.2	D14
HCG 90	0.0088	2364	34.0	III	905	I	50.2	T14
HCG 92	0.0215	6119	88.8	II	789, 7924	S	114.4	T14
HCG 97	0.0218	6174	89.6	III	4988	S	57.4	D14
HCG 100	0.0178	4976	72.0	II	6978, 8491	I	45.6	D14
RSCG 17	0.0190	5415	78.4	II	2223	S	30.4	D14

Note. — Columns are: (1) Compact group name; (2) redshift; (3) velocity from NASA Extragalactic Database (NED) relative to the cosmic microwave background velocity (Fixsen et al. 1996); (4) luminosity distance from NED; (5) group evolutionary H I type as measured and defined by Johnson et al. (2007): (I) H I rich ($\log M_{\rm HI}/\log M_{\rm dyn} > 0.9$); (II) intermediate ($\log M_{\rm HI}/\log M_{\rm dyn} = 0.8-0.9$); and (III) H I poor ($\log M_{\rm HI}/\log M_{\rm dyn} < 0.8$); (6) X-ray observations IDs; (7) *Chandra*-ACIS array; (8) exposure time; (9) for further details and references on the X-ray data see these papers: D14 (Desjardins et al. 2014), T14 (Tzanavaris et al. 2014).

Hickson catalog (Mamon 1994; Ribeiro et al. 1998), it has been shown that several characteristic properties of HCG galaxies are comparable to median galaxy values (e.g. surface brightness and linear or angular diameters, Lee et al. 2004, T14)). One of our CGs comes from the catalog of Redshift Survey Compact Groups (RSCGs, Barton et al. 1996). This RSCG is part of a larger sample selected by Walker et al. (2012) to have properties similar to those of HCGs.

Details on the *Swift* and *Spitzer* observations and data for systems in this sample can be found in Tzanavaris et al. (2010) and L15. For *Chandra*/ACIS observations we refer the reader to T14 and Desjardins et al. (2013, 2014).

3. X-RAY DATA ANALYSIS

3.1. *Point source detection and photometry*

The galaxy groups were observed with *Chandra*'s Advanced CCD Imaging Spectrometer (ACIS), either with the back-illuminated S3 CCD or the ACIS-I array. The data reduction and analysis, as well as point source detection, for CGs labelled T14 in Table 1, Column 6, was done as described in T14. For the rest of the CGs, the data reduction and analysis was carried out using the CIAO 4.5[11] *Chandra* X-ray Center data reduction and analysis suite. Standard aspect solution and grade filtering was used, leading to the production of a final level 2 events file. In the case of multiple observations, observations were reprojected and individual exposure maps created for each observation, before obtaining summed counts and exposure map images (`merge_obs` in CIAO).

Chandra has an unprecedented angular resolution that makes it the instrument of choice for X-ray point source detection. However, this resolution (or, equivalently, the *Chandra* point spread function, PSF) varies across the ACIS CCDs from less than one arcsecond near the aim point to several arcseconds near the CCD edges. Information about this variation must be taken into account before reliable point source detection and characterization can be carried out. For each observation we thus constructed PSF maps (`mkpsfmap` in CIAO) and in the case of multiple observations we also produced a final exposure-weighted mean PSF map.

The PSF map information was used as input at the next stage where we carried out point source detection by correlating the data with wavelet functions (wavdetect in CIAO, Freeman et al. 2002) in the 0.5–8.0 keV energy band. Below 0.5 keV the response is not well calibrated, while above 8.0 keV both the mirror effective area drops and the particle background rises. The false-probability threshold (10^{-6} and 2.4×10^{-7}, for S3 and I0-I3, respectively) was chosen to match the inverse of the size of the chip field, i.e. 1024×1024 pixels for chip S3 and 2048×2048 pixels for chips I0-I3. To cover a broad range of source sizes, and account for the varying point spread function (PSF) size across the ACIS CCD, wavelet scales of 1, 1.414, 2, 2.828, 4, 5.657 and 8.0 pixels were used. This stage produced catalogs of *candidate* point sources.

Each candidate point source has an elliptical source-region assigned to it, for which the local PSF size has been taken into account. We multiplied the ellipse axes by a factor of five and excluded the source region to construct background annuli. These were also checked visually and any non-background emission was further excluded. Net counts were calculated by subtracting area-normalized background counts from source counts. Sources with zero or negative net counts were discarded as non-detections. Poisson $\pm1\sigma$ errors on net counts were estimated by using the method of Gehrels (1986). Sources were also considered as non-detections and discarded if the net counts, after subtraction of the lower 2σ error, were negative. Finally, for detected sources we extracted spectra and associated ancillary response and

[11] http://cxc.harvard.edu/ciao

TABLE 2
X-RAY LUMINOSITIES USED IN THIS PAPER

Name	Description
$L_{X,\rm point}$	X-ray luminosity of a single detected point source.
L_X	Galaxy wide X-ray luminosity from sum of $L_{X,\rm point}$ values within a galaxy region.
$L_{X,\rm gal}$	Galaxy wide X-ray luminosity based on total counts within a galaxy region.

response matrix files (ARF and RMF, `specextract` in CIAO).

3.2. *X-ray luminosities*

In this paper we calculate and/or refer to several different types of X-ray luminosities, a summary of which is presented in Table 2. We further discuss these below.

3.2.1. *Point sources*

Because the majority of point sources have few net counts, reliable spectral fitting cannot be carried out. Instead, as in T14, we estimate X-ray spectral shapes, fluxes and luminosities following Gallagher et al. (2005). If H and S are net counts in the hard $(2.0-8.0$ keV) and soft $(0.5-2.0$ keV) bands, respectively, the hardness ratio is given by $\mathrm{HR} \equiv (H-S)/(H+S)$. For each X-ray point source we compare the observed hardness ratio to that obtained from simulated spectra, and estimate the power-law index Γ (where the photon flux is $f_E \propto E^{-\Gamma}$ photon cm^{-2} s^{-1} keV^{-1}) and corresponding X-ray flux and luminosity.

We produce a set of simulated spectra with XSPEC (Arnaud 1996), version 12.8.1g, for each point source, using the corresponding Galactic column density, $N_{\rm H}^{\rm gal}$, as well as the ARFs and RMFs from the spectral extraction. Each set of spectra uses an absorbed power law model (`tbabs*po` in XSPEC) with Γ varying between -1 and $+4$, giving simulated count rates in the soft and hard band, from which simulated HR values follow. By comparing the observed HR from net counts for each observed detected source within the source extraction region with the simulated HR values, we estimate the best Γ value, and, thus, corresponding flux and point-source luminosity, $L_{X,\rm point}$, for a given X-ray point source.

As the assumed model is simple and assumes no intrinsic absorption ($N_{\rm H}^{\rm int}=0$), some Γ values may in fact be erroneous. However, there is a degeneracy between Γ and $N_{\rm H}$, so that such errors should not affect luminosity values, which is our ultimate goal.

3.2.2. *Galaxy wide*

For each galaxy, we calculate the total X-ray luminosity that is due to point sources, L_X, by first identifying detected point sources that fall within the boundaries of a given galaxy, and then simply summing individual $L_{X,\rm point}$ values, i.e.

$$L_X = \sum_{\rm gal} L_{X,\rm point} \ . \qquad (1)$$

Galaxy boundaries are Kron apertures (Kron 1980) obtained by running SEXtractor (Bertin & Arnouts 1996) on the *Spitzer*/IRAC 3.6μm images, which are the best tracers of stellar mass among our multiwavelength data.

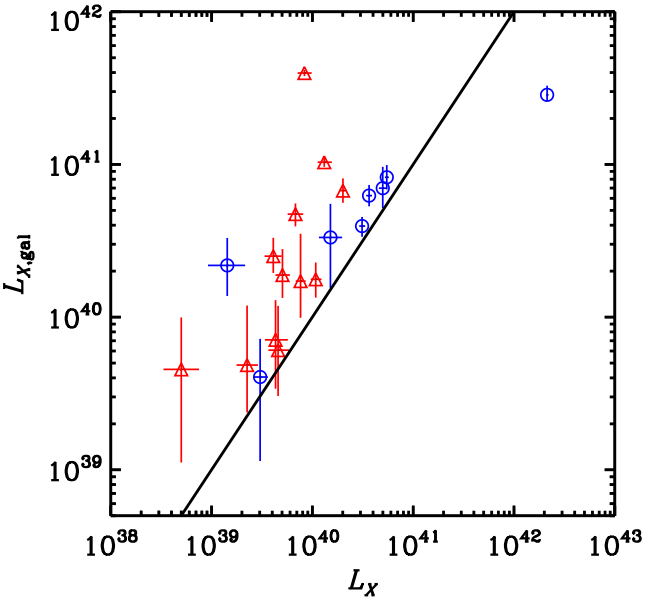

FIG. 1.— "Galaxy-wide" luminosity, $L_{X,\rm gal}$, against total point-source luminosity, $L_{X,\rm gal,p}$, for a sub-sample of our CG galaxies. Blue circles are late types and red triangles early types. The solid line is the equality locus. The source at top right is HCG 92C for which the nuclear emission has been subtracted in the $L_{X,\rm gal}$ estimate. As expected, $L_{X,\rm gal}$ overestimates L_X.

However, it is not always possible to define a single aperture for a galaxy, e.g. in cases of strongly interacting systems. We use a single, combined region for such cases (see L15 for more details). Thus, in this paper the term "galaxy" or "galaxy region" refers to these Kron apertures, which in some cases include more than one letter-designated galaxy.

Some studies in the literature report total galaxy X-ray luminosities calculated from the total X-ray emission within galaxy regions, rather than X-ray emission due only to point sources. If individually detected point sources are not used, a calculated galaxy-wide X-ray luminosity will not necessarily reflect the level of emission due to LMXBs and HMXBs. For the purpose of comparison with such work, we also calculate galaxy-wide luminosities by extracting a single source and background X-ray spectrum for each Kron aperture associated with a CG galaxy. We use XSPEC to fit each spectrum with a power law+thermal plasma, taking Galactic column density into account. For further details, we refer the reader to Desjardins et al. (2015, in prep.). In this paper, we label luminosities derived in this fashion $L_{X,\rm gal}$, to distinguish them from the total point source luminosity inside a galaxy region, L_X. As a sanity check, we compare the two types of luminosities in Fig. 1, where we plot $L_{X,\rm gal}$ against L_X in the 0.5 – 8.0 keV band. As expected, galaxy-wide luminosities from total X-ray emission are consistently higher, with the exception of HCG 92C where the central AGN has been excised by Desjardins et al. (2015). We only show galaxies that are truly single systems (i.e. each region corresponds to a single letter-designated galaxy), but including multiple-galaxy systems doesn't change the result.

3.2.3. *Nuclear Point Sources and Local AGN Contamination*

X-ray point sources located at galaxy centers represent an additional complication for this work. Such sources may be due either to nuclear star clusters or an AGN. If the X-ray luminosity is high ($\gtrsim 10^{41}$ erg s^{-1}) it is highly probable that one is dealing with an AGN. Otherwise, as discussed at length in T14, a variety of multi-wavelength diagnostics may be used to identify the nature of the source. Since we are interested in galaxy-wide X-ray luminosities that originate in XRBs, we identify all nuclear sources either by using the earlier results of T14 or, for galaxies not analyzed in that work, by cross-correlating the *Chandra*/ACIS and *Swift*/UVOT data. We find that 36 out of a total of 47 galaxies (77%) have a nuclear source. Out of these, multiwavelength work has already classified those in the late-type galaxies HCG 16B and 92C, as well as the early-type HCG 22A as AGNs. HCG 16A is classified as LINER or weak AGN by T14. We also tentatively classify the nuclei of RSCGs 17A and 17B as likely AGNs, since the X-ray luminosity is higher than the threshold above. For the remaining galaxies the multiwavelength classification is either non-AGN or unknown. We note that for 12 galaxies (25%) their single X-ray point source is also nuclear. For all galaxies with nuclear X-ray sources we give the fraction of the total luminosity that originates in the nuclear source in column 7 of Table 3.

Overall, we may conservatively assume that a galaxy that fulfills any of three criteria may suffer some AGN contamination: $L_X \geq 10^{41}$ erg s^{-1}, a single nuclear X-ray source or independent AGN classification. There are 15 CG galaxies ($\sim 32\%$) that fulfill at least one of these criteria: Five late-types and ten early-types. These are indicated by red circles in Fig. 2 and Fig. 3.

3.2.4. *X-ray luminosity error*

The error bars associated with X-ray luminosity data points in our figures represent the observational error due to Poisson statistics. However, Gilfanov et al. (2004b) have shown that in the low SFR regime with small numbers of individual X-ray point sources, stochastic effects can be important, leading to an X-ray luminosity excess with respect to the L_X - SFR correlation. Since in general the galaxies in our sample have low SFRs and contain few point sources, we investigate stochastic effects as follows.

For each galaxy and associated luminosity limit (Sec. 3.3) we calculate the total number of point sources that we expect to detect, $< N >$, by integrating the XRB X-ray luminosity functions (XLFs) of Gilfanov (2004) and M12 for early- and late-type galaxies, respectively. For each $< N >$ we carry out 10,000 Monte Carlo (MC) realizations by drawing a number N from a Poisson distribution with mean $< N >$. The normalized XLF is a probability distribution, which we use to randomly assign an $L_{X,\rm point}$ value to each of the N sources, and then calculate an L_X value for each galaxy and realization. The fraction of realizations with L_X values equal to or greater than the observationally obtained L_X values for each galaxy is an estimate of the probability, $P_{b,1}$, that one might obtain our observed L_X values stochastically.

Additionally, both HMXBs and LMXBs may be highly variable, which would exacerbate the issue of small number statistics. The range of possible X-ray luminosities depends on individual characteristics of each XRB system such as accretor and donor type, and transient or persistent emission. On the other hand, it has been suggested that the XRB XLFs are robust against variability (Fabbiano 2006, and references therein). As we do not have specific information for the particular XRB types that we observe, we treat each initial $L_{X,\rm point}$ value in each of our MC realizations, effectively drawn from the corresponding XLF, as a mean value, and assume a variability-driven uncertainty of an order of magnitude above and below this value. We then randomly draw a final $L_{X,\rm point}$ value for each source before calculating L_X for each realization and computing the probability, $P_{b,2}$, that one might obtain our observed L_X values stochastically.

The probabilities $P_{b,1}$ and $P_{b,2}$ are shown in columns 11 and 12 of Table 3. The $P_{b,1}$ values are generally low, with only three out of 47 galaxies ($\sim 6\%$) having $P_{b,1} \geq 0.05$. Thus, if variability is neglected, our L_X values are stochastically improbable. The three galaxies are the late types HCGs 22C, 40BCE and 59A, which agree closely with the M12 L_X-SFR correlation (Sec. 5.1, Table 4 and Fig. 2). This is consistent with the fact that the $P_{b,1}$ estimate assumes the M12 XLF for late type galaxies. As one might expect, $P_{b,2}$ values are often higher. About half of all galaxies (26 or $\sim 55\%$) still have $P_{b,2} < 0.05$; 15 galaxies ($\sim 32\%$) have $0.05 \leq P_{b,2} < 0.20$; and 6 galaxies ($\sim 13\%$) have $P_{b,2} \geq 0.20$. $P_{b,1}$ and $P_{b,2}$ are further discussed in Sec. 6.

3.3. *Flux Limits and Background AGN Contamination*

Without spectroscopic redshifts, it is possible that some of the X-ray point sources within CG galaxies are in fact background AGNs. In our case, the problem is exacerbated by the small number of sources detected per galaxy. Following T14, we estimate the level of background AGN contamination as follows.

We first estimate flux and luminosity limits for our sources. According to (Broos et al. 2010), the binomial probability, P_B for a source to be spurious is given by the binomial function

$$P_B = f_b(C_s; C_s + C_b, (1 + A_b/A_s)^{-1}) \ , \qquad (2)$$

where C_s and C_b are the number of counts observed in the source and background region in a specific energy band, and A_s, A_b are the areas of the source and background regions. Thus, if a source has a value of P_B *less* than some given threshold value, it is considered a detection. We choose the threshold $P_B = 0.004$ determined by Xue et al. (2011) together with local-background count numbers for each detected source to establish a detectability limit in terms of counts, fluxes and luminosities in the $0.5 - 8.0$ keV band at the specific CCD location of each source. Because the calculation of background counts for each source has taken into account the correct local size of the *Chandra* PSF, the calculated detection limits are specific to each source. In our case, C_b is simply the measured background counts for each source. Starting with $C_s = 0$, corresponding to $P_B >> 0.004$ and a clearly spurious source, we increment C_s until a value $C_{s,\rm lim}$ is obtained, corresponding to the chosen P_B threshold of 0.004. Converting the estimated $C_{s,\rm lim}$ value to a flux by assuming a power law spectrum

with $\Gamma = 1.4$ (Hickox & Markevitch 2006; Steffen et al. 2007) and the Galactic N_H value for the host galaxy in PIMMS (Mukai 1993) produces a detection flux limit for the location of a source. Where there are several sources per galaxy we take the lowest source-specific flux limit as the nominal flux limit for the galaxy. The flux and corresponding luminosity detection limits thus obtained are shown in columns 8 and 9 of Table 3.

These flux limits can tell us what is the number of background AGNs we expect to see inside the regions of the CG galaxies. The "$\log N - \log S$" relation of Cappelluti et al. (2009) gives the number of detected X-ray point sources per angular area as a function of flux, established over 2 deg^2 in the COSMOS field. Using our flux limits and this function, we calculate how many background AGNs we would expect to detect in total in our galaxy regions. A measure of the probability $P_{\rm CG}$ (column 10 in Table 3) that a source detected inside a galaxy region is not a background AGN is obtained if we subtract the number of expected AGNs from the number of observed sources and then divide by the number of observed sources. According to Table 3, for 41 out of 47 galaxies (87%), $P_{\rm CG} \geq 0.8$. For the remaining six galaxies (13%), three have $P_{\rm CG} = 0.7$ and three $P_{\rm CG} \leq 0.6$. We are thus confident that the great majority of our sources most likely belong to their associated CG galaxies and, overall, background contamination should not be a major concern for this work. In what follows we always flag the six galaxies with $P_{\rm CG} <= 0.7$ to take into account this relatively higher probability of AGN contamination for X-ray point sources in these galaxies.

4. SFR AND M_*

We obtain SFR and M_* values for our CG galaxies as explained in detail in L15.

Since the SFRs are of particular significance for the conclusions of this paper, we present here the key aspects in their derivation. The SFRs are calculated by combining UV (*Swift*/UVOT 2000Å) and IR (*Spitzer*/MIPS 24μm) photometry, performed inside galaxy boundaries, which are Kron-aperture based (the same as in Sec. 3.2.2), ensuring that $> 90\%$ of the galaxy light is included. All regions have been visually checked, and any contaminating flux from foreground stars or background galaxies has been excluded. Because of the relatively quiescent nature of our galaxies in the low-SFR regime, populations of evolved stars may contribute significantly both in the UV and at 24μm. The UV and 24μm photometry has been corrected for this effect by following the method of Ford et al. (2013). These authors use the UV-to-3.6μm and 24μm-to-3.6μm ratios established for elliptical galaxies (Leroy et al. 2008), to remove the best estimate of UV or 24μm flux not originating from star formation.

Since the UV is a direct tracer of emission from massive O and B stellar populations, while the 24μm traces such emission reprocessed by dust, our SFRs effectively include a correction for intrinsic extinction. To convert luminosities to SFRs the Kennicutt (1998) calibration is used in the UV, and the Rieke et al. (2009) calibration in the IR (appropriate for the luminosity range of our galaxies), leading to the combined SFR determination

$$\begin{aligned}\mathrm{SFR}(M_\odot \mathrm{yr}^{-1}) = {} & 9.5 \times 10^{-44} L_{2000\text{Å}}(\mathrm{ergs}^{-1}) \\ & + 2.0 \times 10^{-43} L_{24\mu\mathrm{m}}(\mathrm{ergs}^{-1}) \,. \end{aligned} \quad (3)$$

As a check, this relation is consistent with the more recent results of Hao et al. (2011), obtained entirely independently from those of Kennicutt (1998) and Rieke et al. (2009). These authors cross-calibrate several multi-wavelength SFR estimators for star-forming galaxies, including near-UV+25μm. The latter combination, which corresponds closely to our wavebands, leads to

$$\begin{aligned}\mathrm{SFR}(M_\odot \mathrm{yr}^{-1}) = {} & 1.1 \times 10^{-43} L_{2000\text{Å}}(\mathrm{ergs}^{-1}) \\ & + 2.4 \times 10^{-43} L_{25\mu\mathrm{m}}(\mathrm{ergs}^{-1}) \,. \end{aligned} \quad (4)$$

Using relation (4) instead of (3) for our galaxies, would lead to an average fractional increase in SFR of 13%, the maximum increase being 15%.

For stellar masses, we follow Eskew et al. (2012), who derive

$$M_* = 10^{5.65} F_{3.6}^{2.85} F_{4.5}^{-1.85} (D/0.05)^2 \quad , \quad (5)$$

where $F_{3.6}$ and $F_{4.5}$ are *Spitzer*/IRAC 3.6 and 4.5μm fluxes, and D distance in Mpc.

5. RESULTS

Table 3 presents star formation rates, stellar masses and total point-source luminosities (L_X) for galaxies in our sample. Other relevant quantities are also included as explained earlier. We now present these results within the context of X-ray scaling relations obtained independently for non-CG environments. A further overview of these results is provided in Tables 4 and 5 for late and early-type galaxies, respectively. In these tables galaxies which show an "excess", a "deficit", or neither because they are within the $\pm 1\sigma$ scatter of a known, non-CG, correlation are labelled **E**, **D** or n, respectively. For each galaxy we also indicate whether there is evidence for a "strong" interaction. We use two main criteria to classify a galaxy as strongly interacting: First, as already mentioned, some Kron galaxy regions contain more than one letter-designated system (e.g. HCG 31 ACE). Such multi-galaxy systems show pronounced morphological distortions and tidal features, which are the signatures of active interaction and merging. Using the classification scheme of Surace et al. (1998) (see also Veilleux et al. 2002), such interactions are at least type II ("First contact"), where there is clear overlap. Second, for a subset of our data, the level of interaction has been studied in detail by means of kinematic, Fabry-Perot, data, and specific interaction indicators (Plana et al. 1998; Mendes de Oliveira et al. 1998, 2003; Amram et al. 2004; Torres-Flores et al. 2009, 2010, 2014). These indicators include a highly disturbed velocity field, central double nuclei, double kinematic gas component (i.e. a disagreement between both sides of the rotation curve), kinematic warping, gaseous vs. stellar major-axis misalignment (hereafter, G/SMM), tidal tails, high IR luminosity and central activity. As discussed by Mendes de Oliveira et al. (1998, herafter M98), the first three are most definitely associated with mergers.

TABLE 3
CG Galaxy Results

ID	Morphology	SFR $M_\odot \mathrm{yr}^{-1}$	M_* $10^{10} M_\odot$	L_X $10^{40}\mathrm{erg\ s}^{-1}$	Number of sources	central L_X fraction	f_{lim} 10^{-15} erg cm^{-2} s^{-1}	$L_{X,\mathrm{lim}}$ $10^{38}\mathrm{erg\ s}^{-1}$	P_{CG}	$P_{b,1}$	$P_{b,2}$
(1)	(2)	(3)	(4)	(5)	(6)	(7)	(8)	(9)	(10)	(11)	(12)
H 7A	S	3.41 ± 0.45	9.17 ± 0.04	$3.65^{+0.25}_{-0.23}$	2	0.27	2.2	8.3	0.6	0.01	0.17
H 7B	S0	0.23 ± 0.03	4.65 ± 0.05	$0.22^{+0.06}_{-0.05}$	2	0.45	1.0	3.6	0.5	0.00	0.28
H 7C	S	2.00 ± 0.23	4.51 ± 0.04	$5.47^{+0.25}_{-0.23}$	6	0.02	1.6	6.0	0.9	0.00	0.05
H 7D	S0	0.43 ± 0.05	1.37 ± 0.06	$0.76^{+0.09}_{-0.08}$	2	...	1.0	3.6	0.6	0.00	0.01
H 16A	S	4.65 ± 0.60	10.50 ± 0.04	$4.99^{+0.46}_{-0.42}$	2	0.94	7.3	24.8	0.9	0.01	0.15
H 16B	S	0.48 ± 0.06	6.41 ± 0.04	$22.00^{+1.70}_{-1.60}$	1	1.00	7.3	24.8	0.9	0.00	0.00
H 16C	S0	13.98 ± 1.85	6.74 ± 0.03	$1.31^{+0.25}_{-0.18}$	4	0.40	4.5	15.5	0.9	0.00	0.00
H 16D	S0	16.73 ± 2.26	3.79 ± 0.02	$0.68^{+0.13}_{-0.11}$	1	1.00	5.4	18.6	0.8	0.00	0.00
H 22A	E	0.36 ± 0.04	9.14 ± 0.02	$1.08^{+0.15}_{-0.12}$	12	0.05	1.1	1.7	0.8	0.00	0.35
H 22B	S0	0.06 ± 0.01	0.76 ± 0.03	$0.05^{+0.02}_{-0.02}$	1	1.00	1.4	2.3	0.7	0.04	0.11
H 22C	S	0.55 ± 0.06	0.80 ± 0.02	$0.30^{+0.06}_{-0.04}$	3	...	1.4	2.3	0.7	0.08	0.17
H 31ACE	S	9.93 ± 1.17	2.27 ± 0.04	$9.60^{+0.44}_{-0.39}$	9	0.23	1.0	3.9	0.9	0.01	0.28
H 31B	S	1.06 ± 0.11	0.36 ± 0.20	$2.11^{+0.22}_{-0.19}$	3	...	1.3	5.2	1.0	0.01	0.09
H 31G	S	1.83 ± 0.20	0.71 ± 0.10	$3.11^{+0.23}_{-0.20}$	5	0.31	1.3	5.2	1.0	0.01	0.08
H 31Q	Im	0.13 ± 0.02	0.20 ± 0.37	$0.08^{+0.05}_{-0.04}$	1	...	1.0	3.9	1.0	0.01	0.02
H 37A	E	0.87 ± 0.12	27.40 ± 0.16	$3.83^{+0.47}_{-0.42}$	1	1.00	9.0	98.4	1.0	0.00	0.00
H 37B	S	1.27 ± 0.17	10.70 ± 0.15	$1.48^{+0.50}_{-0.38}$	1	...	1.9	21.2	0.9	0.01	0.06
H 37C	S	0.14 ± 0.06	2.74 ± 0.46	$1.18^{+0.53}_{-0.35}$	2	0.62	1.9	21.2	1.0	0.00	0.00
H 40A	E	0.69 ± 0.09	22.00 ± 0.16	$0.48^{+0.12}_{-0.09}$	1	1.00	1.7	18.4	0.9	0.00	0.00
H 40BCE	S	3.16 ± 0.41	20.50 ± 0.14	$1.81^{+0.34}_{-0.27}$	2	0.85	1.2	13.1	0.7	0.05	0.25
H 40D	S0	3.65 ± 0.48	9.88 ± 0.14	$1.15^{+0.16}_{-0.14}$	2	0.40	3.4	36.7	1.0	0.00	0.00
H 42A	E	0.71 ± 0.08	31.90 ± 0.06	$1.78^{+0.14}_{-0.13}$	1	1.00	13.7	64.2	0.8	0.00	0.00
H 42B	S0	0.20 ± 0.04	4.76 ± 0.06	$0.43^{+0.14}_{-0.09}$	3	...	1.1	5.1	0.8	0.00	0.06
H 42C	E	0.14 ± 0.04	4.71 ± 0.06	$0.30^{+0.08}_{-0.06}$	2	0.71	4.7	22.0	0.8	0.00	0.00
H 42D	S0	0.02 ± 0.01	1.08 ± 0.21	$0.33^{+0.13}_{-0.09}$	2	...	1.4	6.8	1.0	0.00	0.00
H 59A	S	5.92 ± 0.80	1.48 ± 0.04	$1.36^{+0.24}_{-0.20}$	1	1.00	1.8	8.6	0.8	0.24	0.63
H 59B	E	0.03 ± 0.00	0.94 ± 0.17	$0.46^{+0.13}_{-0.09}$	3	0.48	0.9	4.3	1.0	0.00	0.01
H 59C	S	0.19 ± 0.04	0.41 ± 0.29	$0.91^{+0.22}_{-0.17}$	2	...	0.9	4.3	0.9	0.00	0.01
H 62A	S0	0.63 ± 0.08	16.60 ± 0.07	$3.70^{+0.13}_{-0.11}$	13	0.09	2.0	10.1	1.0	0.00	0.00
H 62B	S0	0.28 ± 0.04	9.21 ± 0.07	$0.64^{+0.05}_{-0.04}$	4	0.43	2.0	10.1	0.9	0.00	0.00
H 62C	S0	0.14 ± 0.03	3.57 ± 0.06	$0.83^{+0.10}_{-0.07}$	9	0.13	0.7	3.4	0.9	0.00	0.03
H 62D	S0	0.06 ± 0.02	1.18 ± 0.23	$0.27^{+0.07}_{-0.06}$	1	...	2.1	10.4	0.9	0.00	0.00
H 79AD	S	0.78 ± 0.09	4.29 ± 0.06	$1.29^{+0.15}_{-0.12}$	4	...	0.5	2.3	0.8	0.01	0.08
H 79BC	S0	0.87 ± 0.11	6.07 ± 0.06	$0.43^{+0.08}_{-0.06}$	3	0.35	1.2	5.4	0.8	0.00	0.07
H 90BD	S	1.09 ± 0.14	12.70 ± 0.02	$0.93^{+0.09}_{-0.07}$	14	0.13	0.9	1.2	0.9	0.04	0.15
H 90C	E	0.11 ± 0.01	4.52 ± 0.02	$0.59^{+0.09}_{-0.07}$	10	0.20	0.9	1.2	1.0	0.00	0.20
H 92B	S	1.73 ± 0.19	14.50 ± 0.18	$1.61^{+0.18}_{-0.13}$	12	0.15	0.5	4.8	1.0	0.03	0.15
H 92C	S	5.19 ± 0.69	8.82 ± 0.07	$213.00^{+4.01}_{-3.01}$	6	0.99	0.6	5.8	1.0	0.00	0.00
H 92D	E	1.56 ± 0.19	17.60 ± 0.18	$8.15^{+0.35}_{-0.32}$	6	0.08	0.5	4.8	1.0	0.00	0.00
H 92E	E	0.37 ± 0.06	11.00 ± 0.14	$0.51^{+0.09}_{-0.08}$	2	0.79	0.7	6.7	0.9	0.00	0.04
H 97A	S0	0.34 ± 0.07	13.20 ± 0.11	$0.83^{+0.15}_{-0.12}$	2	0.49	2.2	22.9	0.9	0.00	0.00
H 97D	E	0.36 ± 0.07	12.00 ± 0.11	$2.01^{+0.17}_{-0.16}$	1	1.00	4.2	43.6	1.0	0.00	0.00
H 100A	S	3.49 ± 0.44	8.30 ± 0.07	$2.95^{+0.50}_{-0.43}$	2	...	2.6	18.3	1.0	0.02	0.18
H 100B	S	1.30 ± 0.15	4.49 ± 0.08	$1.51^{+0.46}_{-0.35}$	1	1.00	2.0	13.8	1.0	0.02	0.09
R 17A	E	0.66 ± 0.09	32.50 ± 0.10	$10.80^{+0.40}_{-0.40}$	1	1.00	41.2	326.0	1.0	0.00	0.00
R 17B	E	0.31 ± 0.04	8.08 ± 0.09	$13.20^{+0.50}_{-0.50}$	1	1.00	4.6	36.3	1.0	0.00	0.00
R 17C	E	0.19 ± 0.04	3.98 ± 0.13	$0.41^{+0.09}_{-0.07}$	1	1.00	5.0	39.3	1.0	0.00	0.00

Note. — Columns are (1) galaxy ID (H for HCG, R for RSCG); (2) morphology based on best-fitting SED template (see L15 for details); (3) star formation rate; (4) stellar mass in units of 10^{10} solar masses; (5) total X-ray luminosity from point sources within a galaxy region in units of $10^{40}\mathrm{erg\ s}^{-1}$ in the 0.5-8.0 keV *Chandra* band; (6) number of detected point sources; (7) if there is a central source, fraction of the total luminosity contributed by the central source; (8) flux limit in units of 10^{-15} erg cm^{-2} s^{-1}; (9) $0.5-8.0$ keV luminosity limit in units of 10^{38} erg s^{-1}; (10) probability that a source detected within the galaxy boundaries belongs to the CG galaxy; (11) probability of measuring a total galaxy luminosity greater than or equal to the observed value, given the luminosity detection limit for the galaxy and the Gilfanov (2004) or Mineo et al. (2012) XRB XLFs; (12) as (11), but also assuming a range in luminosity for individual point sources of two orders of magnitude to account for variability.

TABLE 4
CGs and Late-type Galaxy Correlations

ID	L_X-SFR	Strong interaction?	Comments
(1)	(2)	(3)	(4)
16B	**E**	✓	Strong AGN; interacting with A; G/SMM (M98). Single nuclear source.
92C	**E**	✓	Strong AGN; tidal tails (TF09).
37C	**E**	✓	Interacting with H37A.
59C	**E**		
31B	**E**	✓	Interacting with ACE.
7C	**E**	✓	Nuclear ring.
31G	**E**	✓	Peculiar morphology.
79AD	**E**	✓	Peculiar morphology.
37B	**E**		
100B	**E**	✓	Several signs of kinematic disturbance (Plana et al. 2003).
16A	**E**	✓	Possible LINER/weak AGN (T14, O'Sullivan et al. 2014b,a); interacting with H16B (bridge of diffuse emission, Jeltema et al. 2008).
7A	**E**	✓	Disturbed velocity field (TF09).
31ACE	**E**	✓	Wolf-Rayet starburst interacting complex (López-Sánchez et al. 2004).
92B	**E**	✓	Unresolved X-ray emission. Tidal tails (TF09).
90BD	**E**	✓	Unresolved X-ray emission. Kinematically disturbed (Plana et al. 1998).
100A	**E**		
31Q	n		Most isolated HCG31 galaxy.
40BCE	n	✓	Only two point sources. G/SMM in 40E (Torres-Flores et al. 2010).
22C	n		
59A	n		TO/LINER (T14).

Note. — Columns are: (1) Spiral/irregular CG galaxies listed from top to bottom in order of *decreasing excess* relative to the M12 correlation (galaxies are HCGs except for designations starting with an R which are RSCGs); (2) excess (**E**), Deficit (**D**), or none (n) relative to the M12 correlation; (4) evidence of strong interaction.

5.1. L_X *vs. SFR*

In Fig. 2 we plot L_X against SFR for late-type galaxies in this sample, together with the M12 best fit and $\pm1\sigma$ scatter, and the comparison samples of Douna et al. (2015) and Basu-Zych et al. (2013) (see Section 6). Four galaxies are within the correlation's scatter, while the remaining 16 (80%) show an "excess" (higher scatter). Specifically:

1. In order of decreasing "excess" the 16 "extreme L_X" galaxies are:
   - The two known *strong* X-ray AGNs HCG 16B (O'Sullivan et al. 2014b,a) and HCG 92C (NGC 7319). The former is a single nuclear X-ray point source. As shown in T14 the CG environment is very rarely host to unambiguously strong nuclear AGN emission; for this reason we have not attempted to exclude nuclear point-source emission in this work. These are the only late types in our sample that are strong AGNs, clearly the primary cause of the observed excess. HCG 16B is also strongly interacting with its neighbor 16A (classification LINER/weak AGN in T14), to which it is linked by a bridge of diffuse (X-ray and optical) emission (Jeltema et al. 2008). The Fabry-Perot analysis of M98 detects a highly disturbed velocity field in HCG 16B, kinematic warping and G/SMM. Similar analysis for 92C (NGC 7319) also detects prominent tidal tails (Torres-Flores et al. 2009, hereafter TF09).
   - HCGs 37C and 59C, which are both classified star-forming (morphologies S? in de Vaucouleurs et al. 1991). The first is strongly interacting with HCG 37A. There is no evidence for interactions for 59C (Konstantopoulos et al. 2012).
   - HCG 31B, interacting with the merging ACE complex.
   - HCG 7C, which has a nuclear ring.
   - HCG 31G, morphologically peculiar.
   - The pair HCG 79AD, morphologically classified peculiar, with a peculiar velocity field and highly interacting (Mendes de Oliveira et al. 2003)).
   - HCG 37B.
   - HCG 100B of morphology S? and very strongly interacting with its neighbors as shown by Plana et al. (2003, highly disturbed velocity field, double nuclei, tidal tails).
   - HCG 16A (candidate LINER or weak AGN in T14, tidal tails in M98, close to an intergalactic H II region, Werk et al. (2010)).
   - HCG 7A (highly disturbed velocity field, TF09).
   - HCG 31ACE (a highly interacting merging complex classified a Wolf-Rayet starburst).
   - HCG 92B (NGC 7318B), for which tidal tails were detected by TF09.
   - HCG 90BD (highly interacting (Plana et al. 1998)).
   - HCG 100A.

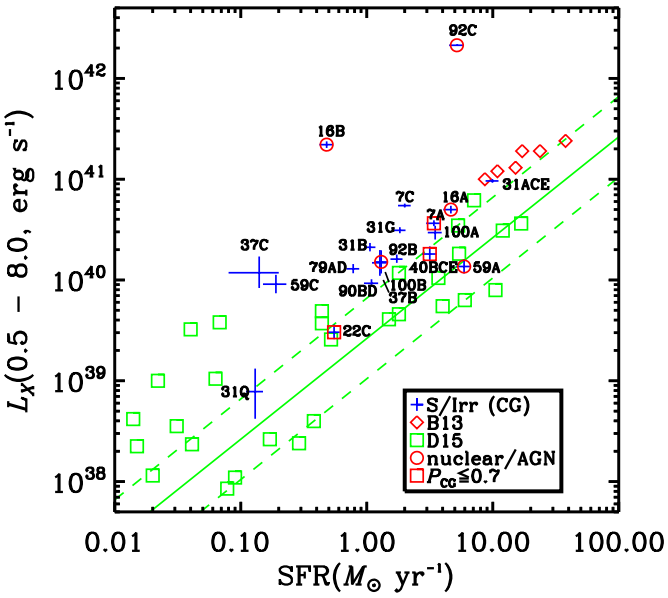

FIG. 2.— Total X-ray luminosity from point sources, L_X, vs. SFR for late-type CG galaxies (blue symbols and error-bars). The five galaxies with a single, nuclear X-ray source and/or known independently to be AGNs and/or having $L_X \geq 10^{41}$ erg s^{-1} are flagged with red circles. The three late-type galaxies with detected sources having a lower probability of belonging to their galaxy (higher probability of being background AGNs) are flagged with red squares. The solid (green) line is the M12 correlation for resolved HMXBs in nearby star-forming galaxies. Its $\pm1\sigma$ scatter is shown with dotted lines. The green squares are the Douna et al. (2015) data (D15) from nearby low-metallicity galaxies. The red diamonds are the Lyman-break galaxies of Basu-Zych et al. (2013, B13). Individual late-type HCG galaxies discussed in the text are indicated.

2. The four galaxies that are within the scatter of the M12 correlation are:
   - HCG 31Q, the most isolated, lowest SFR and L_X galaxy in the otherwise highly active HCG 31 complex.
   - HCG 40BCE, a three galaxy interacting complex, although it shows no disturbed velocity field in Torres-Flores et al. (2010).
   - HCG 22C, for which TF09 do not find a highly disturbed velocity field (they do detect G/SMM).
   - HCG 59A (no evidence of interactions, classified TO/LINER in T14).

5.2. L_X *vs.* M_*

In Figures 3 and 4 we plot L_X against M_* results for early type galaxies, together with the early-type sample of B11. Here, each purple diamond point represents the total X-ray luminosity due to LMXBs for a B11 galaxy. The best-fit and $\pm1\sigma$ scatter are shown by the solid and dotted black lines. The corresponding quantity, L_X, for CG early-types is plotted with red error bars in Fig. 3, which in Fig. 4 are either starred or unstarred, for galaxies of *group* evolutionary types II and III, respectively. Finally, in both figures, the green crosses show the total X-ray luminosity taking into account all types of X-ray emission (i.e. not just LMXBs) in B11 galaxies. It appears that about 50% (13/27) of CG galaxies are within

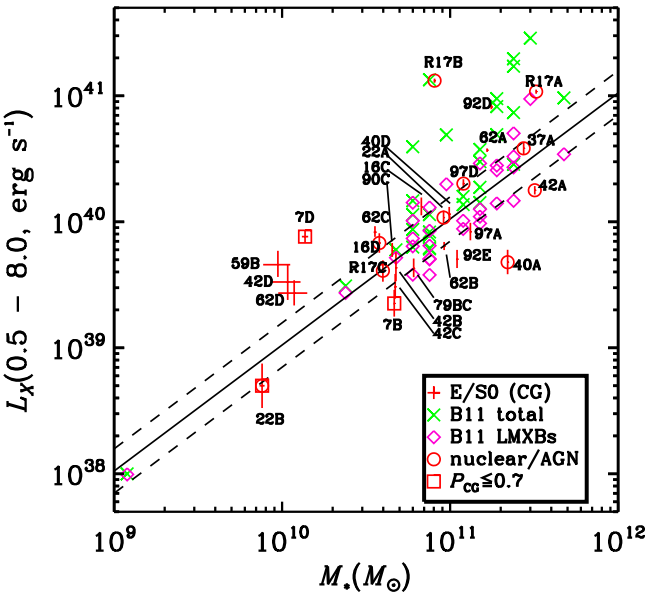

FIG. 3.— Total X-ray luminosity from point sources, L_X, vs. M_* for early type CG galaxies (red symbols and error bars). The ten galaxies with a single, nuclear X-ray source and/or known independently to be AGNs and/or having $L_X \geq 10^{41}$ erg s^{-1} are flagged with red circles. The three galaxies with detected sources having a lower probability of belonging to their galaxy (higher probability of being background AGNs) are flagged with red squares. CG galaxies discussed in the text are labeled. Labels for RSCGs begin with an R, otherwise galaxies are in HCGs. The solid line is the correlation of B11 (with $\pm1\sigma$ scatter dotted lines). Other symbols are: *Green X's:* B11 sample total (LMXB+AB+CV+AGN+hot gas) L_X values; *purple diamonds:* B11 sample L_X values for LMXBs only.

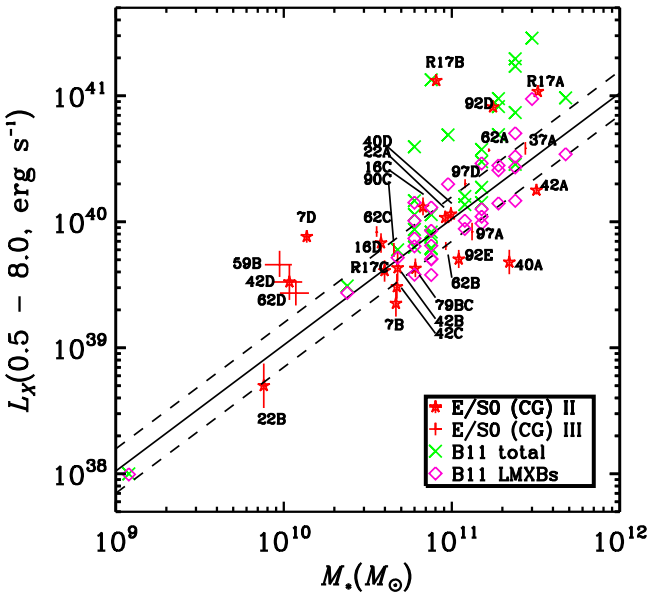

FIG. 4.— Same as Fig. 3, but also showing parent group H I types: Starred symbols are for CG galaxies in groups of evolutionary H I type II; non-starred symbols are for galaxies in groups of evolutionary H I type III (see Table 1 for type definitions).

the scatter of the correlation; the rest have higher scatter, both above and below the best-fit line.

Specifically:

1. Galaxies with higher scatter than the B11 correlation and on the high-L_X side ("excess") include:
   - The interacting pair RSCG 17B and A show the first and fifth highest excess, respectively. For both galaxies, the only X-ray sources are nuclear and dominate the X-ray luminosity at 1.1 and 1.3 $\times$ 10^{41}erg s^{-1}, respectively, making them both candidates for AGN activity.
   - Second comes HCG 7D, with high levels of asymmetric emission both in the UV and in R (Konstantopoulos et al. 2010). TF09 identify a strong G/SMM. However, background AGN contamination is relatively likely for this galaxy ($P_{\rm CG}$ = 0.6). It is followed closely by HCG 59B for which in a deep co-added $B+R$ image Konstantopoulos et al. (2012) detect a string of H II regions to the west of the galaxy, as well as a tidal bridge to neighbor A.
   - HCG 92D (NGC 7318A) is located in a region of Stephan's Quintet which shows several star forming clumps and high-levels of diffuse emission. It shows prominent tidal tails (TF09).
   - HCG 42D is a low-L_X galaxy, that doesn't show any signs of strong interactions (Konstantopoulos et al. 2013).
   - HCGs 62A, and C are closely interacting: A is optically classified TO/LINER? with a radio excess from the radio-SFR correlation (T14). HCG 62D has no obvious interactions but it does show an excess of about the same level as A and C.
   - Finally, HCG 16C, shows several signs of strong interactions (M98): it has a highly disturbed velocity field, central double nuclei, G/SMM, a double kinematic gas component and kinematic warping. It is classified TO/SF in T14.
2. Galaxies within the correlation's $\pm1\sigma$ scatter include:
   - HCG 16D is interacting with neighbor C, with whom it shares some signs of strong interactions (M98) such as peculiar velocity field and double nuclei. This is a single nuclear X-ray source, but the galaxy is optically classified star-forming (T14).
   - HCG 37A, closely interacting with late-type 37C, has a double kinematic gas component (Torres-Flores et al. 2010). It also has a single nuclear X-ray source and no independent nuclear classification.
   - HCG 40D, interacting with 40A.
   - The interacting pair HCG 79BC. The detailed work of Durbala et al. (2008), however, finds no evidence of major mergers[12].

[12] The Fabry-Perot results of these authors are not presented in a way that is directly comparable to those for the rest of the systems.

- HCG 62B, interacting with 62A.
- RSCG 17C and HCGs 22A, 22B, 42B, 42C, 90C, 97A, 97D are not obviously interacting with any neighbors. RSCG 17C, HCGs 22B, 97D are single nuclear sources. HCG 22A is classified AGN (T14). Where available (TF09 for HCG 22A, B; Plana et al. (1998) for HCG 90C) Fabry-Perot kinematic results confirm this: only HCG 90C shows one indicator for interaction, namely G/SMM.

3. Galaxies that fall below the $\pm1\sigma$ scatter bound include:

- HCG 42A, a morphologically smooth elliptical. Single nuclear source and optical classification "non-SF".
- HCG 7B (no obvious interaction; corroborated by kinematic information, TF09). Background AGN contamination is likely ($P_{\rm CG} = 0.5$).
- HCG 92E (NGC 7317), a rare case of a galaxy in Stephan's Quintet away from the "main action". Only one minor kinematic interaction index in TF09.
- HCG 40A, interacting with 40D, although not morphologically disturbed. Single nuclear source.

We note that, as suggested by Fig. 4, there is no indication that the group evolutionary type is a predictor of the location of an early-type CG galaxy in L_X-M_* space.

6. DISCUSSION

Our results suggest that X-ray point sources in CG galaxies show trends that depend on galaxy morphology. Thus, most late-type galaxies show L_X values higher than expected from the M12 correlation and its scatter; the rest appear to be close to the best fit line, with no lower-L_X scatter. In contrast, early-type galaxies are consistent with the B11 correlation but show larger scatter.

It is well established that many of the CG galaxies in this sample are subject to strong interactions with neighbors. The evidence summarized in Tables 4 and 5 suggests that there might exist a connection between excess L_X, as compared to that expected from non-CG environments, and interaction level. However, whatever the physical mechanism behind the observed excesses might be, it is not clear from these data that a high interaction level is either necessary or sufficient to produce L_X excesses. There is an *indication of a trend* for excess L_X to accompany high interaction levels. This is best seen in the case of the excess observed for late-type systems relative to the L_X-SFR relation: Although 13 out of 16 such systems (81%) showing an excess are also strongly interacting (this includes the AGNs), three systems show an excess without clear signs of interactions. Also, one system is strongly interacting but does not show an excess. This may simply be evidence for scatter in the relations combined with small number statistics.

We note that this connection can be investigated further by quantifying interaction level, e.g. according to a scheme that weighs interaction indicators. Unfortunately, for the present sample there are too few systems that have detailed and conclusive kinematic information for one to carry out such an analysis.

Can the observed deviations be due to systematics? For instance, it can be seen from Fig. 2 than an increase by an order of magnitude in SFR would bring late type systems into general agreement with the M12 correlation. The derivation of our SFRs is explained in Sec. 4. As explained there, a recent alternative calibration might at worse increase these values by up to $\sim 13\%$, on average. This is not nearly sufficient to compensate for systems that show excess L_X in Fig. 2. In addition, for a subset of our systems, Bitsakis et al. (2014) have obtained independent estimates using *Herschel* data and UV-to-IR SED fitting. Their SFRs are systematically *lower* than ours, which would make our late-type excesses even more severe. There is thus no evidence that our SFRs are systematically too low, which would lead to an artificial excess in the L_X–SFR relation.

Since our X-ray luminosities are point-source based, it is unlikely that L_X is overestimated due to contamination from diffuse emission. It also seems improbable that, overall, background or nuclear AGN contamination can significantly affect our results. In total, there are 20 late- and 27 early-types in our CG sample. In Figs. 2 and 3 we flag galaxies with a known AGN, a single nuclear source or $L_X \geq 10^{41}$ erg s^{-1} with solid red circles. We also flag galaxies with low $P_{\rm CG}$ values with red squares. Conservatively excluding all these galaxies (eight late-type and twelve early-type), still leaves 11 out of 12 late-type galaxies (92%) with an L_X excess, and 8 out of 15 early-type galaxies (53%) with an L_X excess or deficit. Assuming the M12 and Gilfanov (2004) XRB XLFs, $P_{b,1}$ is less than 0.05 for all but three of these, so stochastic effects do not seem important. On the other hand, as the $P_{b,2}$ values show, if a variability estimate is included, such effects may be more significant for up to $\sim 45\%$ of galaxies. Since many of these galaxies contain nuclear as well as non-nuclear sources, some AGN contamination intrinsic to the galaxies cannot be excluded. The fact that we do not carry out detailed spectral fitting should not affect the actual L_X values. As shown by T14, even if individual Γ values are incorrect, fitted $N_{\rm H}$ and Γ values work together to produce correct X-ray luminosities.

In this work we make the assumption that X-ray point sources in early- and late-type galaxies are LMXBs and HMXBs respectively. In reality, however, it is possible that the L_X value for a galaxy region includes a contribution from XRBs of the "wrong" type, i.e. either LMXBs in early-types or HMXBs in late-types (see Luo et al. 2012, for an example). Since in most cases we only have very few, low-luminosity sources for each galaxy region, this can make a significant difference. Without high spatial resolution multi-wavelength information for each point source we are not able to separate LMXBs from HMXBs. We can however obtain a rough estimate of the total contribution of LMXBs and HMXBs by using the correlations of M12 and B11. We use the M12 correlation and SFRs for early-type galaxies to obtain an estimate for the HMXB contribution in these systems. Similarly, the B11 correlation and M_* in late-type galaxies provide an estimate for the LMXB contribution.

The X's in Figs 5 and 6 show the effect of subtracting these estimated contributions for late- and early-type

TABLE 5
CGs and Early-type Galaxy Correlations

ID	L_X-M_*	Strong interaction?	Comments
(1)	(2)	(3)	(4)
R17B	**E**	✓	Candidate AGN.
7D	**E**	✓	G/SMM (TF09). Possible background AGN contamination.
59B	**E**	✓	Western string of H II regions; tidal bridge to A (Konstantopoulos et al. 2012).
92D	**E**	✓	Prominent tidal tails (TF09) and diffuse emission. Substantial amounts of hot gas due to $M_* > 10^{11} M_\odot$(B11).
R17A	**E**	✓	Candidate AGN. Substantial amounts of hot gas due to $M_* > 10^{11} M_\odot$(B11).
42D	**E**		Low L_X; no signs of interactions.
62C	**E**	✓	Interacting with A.
62D	**E**		
62A	**E**	✓	Interacting with C. TO/LINER? and radio excess (T14). Substantial amounts of hot gas due to $M_* > 10^{11} M_\odot$(B11).
16C	**E**	✓	Several kinematic signs of strong interactions (M98); TO/SF in T14.
16D	n	✓	Interacting with C. Some kinematic interaction indicators (M98). Single nuclear X-ray source, classification SF (T14).
97D	n		
37A	n	✓	Interacting with C. Double kinematic gas component (Torres-Flores et al. 2010). Single nuclear X-ray source.
90C	n		
22A	n		AGN optical classification in T14.
40D	n	✓	Interacting with 40A. G/SMM (TF10).
R17C	n		
42B	n		
79BC	n	✓	Interacting pair.
62B	n	✓	Interacting with 62A.
22B	n		
42C	n		
97A	n		
42A	**D**		Single nuclear X-ray source. Classification "non-SF" (T14).
7B	**D**		Likely background AGN contamination.
92E	**D**		
40A	**D**		Interacting with 40D. Single nuclear X-ray source.

Note. — Columns are: (1) Elliptical/S0 CG galaxies listed from top to bottom in order of *decreasing excess* relative to the B11 correlation (galaxies are HCGs except for designations starting with an R which are RSCGs); (2) excess (**E**), Deficit (**D**), or none (n) relative to the B11 correlation; (3) interaction level from kinematical work in the literature or qualitative interaction indication (✓).

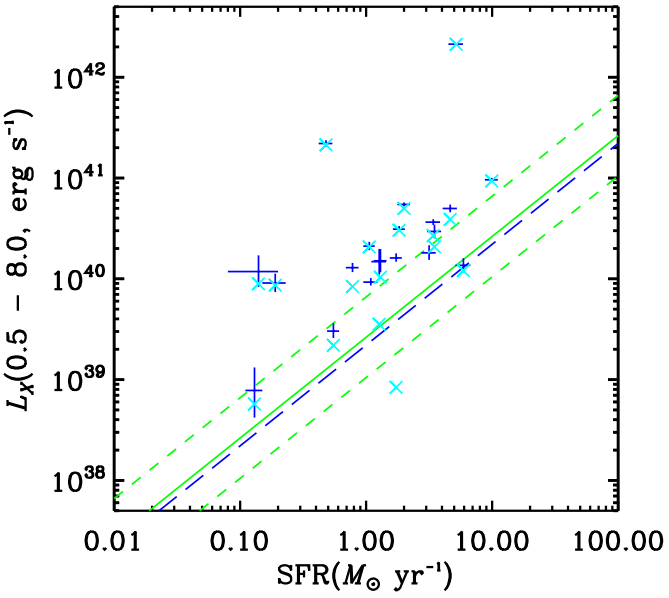

Fig. 5.— Same as Fig. 2 but including effect of subtracting an LMXB contribution, estimated from M_*. The resulting lower L_X values are shown by light-blue X's.

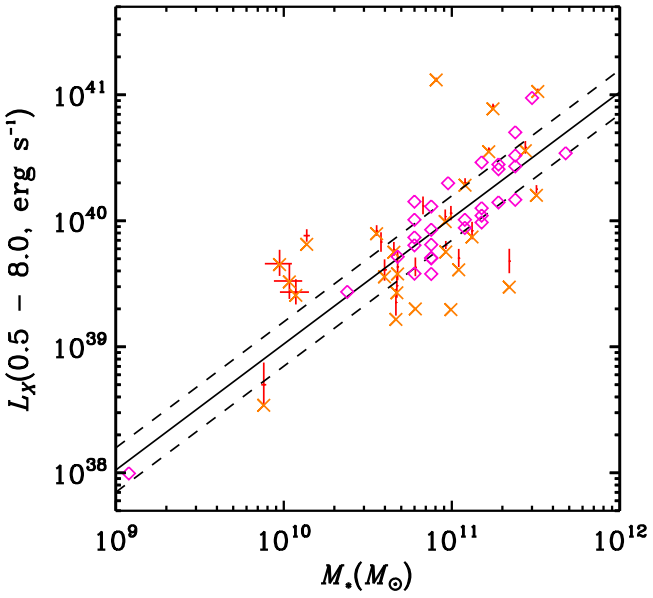

Fig. 6.— Same as Fig. 3 but showing the effect of subtracting a contribution from HMXBs, estimated from the SFR. The resulting lower L_X values are shown by orange X's.

galaxies, respectively. It can be seen that the effect may be significant only for the lowest-luminosity systems. Excesses from the correlations can thus in general not be explained in this way.

For massive ellipticals ($M_* > 10^{11} M_\odot$) B11 further caution that the contribution from hot gas can be significant. If we include S0 types, ten of our early-type galaxies have masses in this range. Since not all show an excess, such a contribution may be relevant to the high L_X values for HCG 62A, HCG 92D (NGC 7318A) and RSCG 17A. It is unlikely that this is a very significant effect, since we are only including emission from point sources.

The X-ray luminosity function of XRBs in CGs is unknown and we have not carried out any incompleteness corrections at the faint end. Significant numbers of undetected and/or unresolved XRBs may further increase excess or decrease deficits.

After taking into account possible AGN contamination (local or background), a number of late-type CG galaxies still show unusually high L_X for their SFRs. It is well known that XRB numbers and luminosities are affected by metallicity (Mapelli et al. 2009; Zampieri & Roberts 2009). XRB population synthesis modeling has shown a significant increase in L_X/SFR with redshift (Fragos et al. 2013; Tremmel et al. 2013; Basu-Zych et al. 2013) where metallicity is lower. Lower metallicities imply weaker stellar winds, resulting in a lower mass loss of XRB primaries and, hence, an increased production of massive black hole (BH) accretors. In turn, BH-XRBs are more luminous than neutron-star (NS) XRBs for two reasons. First, they can form stable Roche lobe overflow systems with high-mass secondaries. Second, BHs have higher mass and higher Eddington limits, thus giving rise to higher accretion rates. In this way, lower metallicities can lead to higher luminosities both for LMXBs and HMXBs.

In Fig. 2 the green squares indicate the total X-ray luminosities from HMXBs in the nearby galaxy sample of Douna et al. (2015). Each luminosity value represents the total from individually detected HMXBs, i.e. is equivalent to our L_X values. These authors have specifically targeted low-metallicity galaxies, showing that there is an excess in HMXB emission at low metallicities ($Z \lesssim 0.2 Z_\odot$). Further, the observed excess tends to increase with decreasing SFR. We also show the local ($z < 0.1$) "Lyman Break Analogs" of Basu-Zych et al. (2013) with red diamonds. These authors find an excess for their systems, which also have sub-solar metallicities ($Z \lesssim 0.6 Z_\odot$). With the exception of our two highest excess systems which are strong AGNs, it is clear that the rest of the late-type CG galaxies occupy a similar locus in L_X-SFR space. Similar to what noted by Douna et al. (2015) there is also evidence for a stronger excess at lower SFR. This is consistent with the reported low metallicities for prominent CG star-forming systems such as HCG 31 ($Z \sim 0.2 Z_\odot$, López-Sánchez et al. 2004; Gallagher et al. 2010) and HCG 92 ($Z \sim 0.2, Z_\odot$ Saracco & Ciliegi 1995; Fedotov et al. 2011).

There are currently no other metallicity measurements for late type CG galaxies that would allow us to verify this low-metallicity interpretation. Using the mass-metallicity relation of Tremonti et al. (2004) leads to estimates of solar metallicities, or higher, for these systems. This, however, is at odds with existing direct measurements, e.g. for HCG 31. CG late-type galaxies are however not typical star-forming galaxies: As mentioned, most are undergoing strong interactions, likely leading to significant gas and metal removal. As a result, although CG galaxies as a class are not dwarfs, their mass-metallicity relation might be more similar to that for dwarf galaxies (Kirby et al. 2013). Formally applying such a relation consistently produces low metallicities, in agreement with the few direct results available at present.

Many of our individual X-ray point sources have luminosities greater than the fiducial threshold of 10^{39}erg s^{-1} and can thus be classified as "Ultra-luminous" (ULXs). Independent evidence exists for increased numbers of ULXs in low-metallicity environments (Swartz et al. 2008; Mapelli et al. 2010; Kaaret et al. 2011; Prestwich et al. 2013) consistent with what we detect here.

Alternatively, and independently of a low-metallicity interpretation, over an extended period in time interactions can trigger and maintain elevated levels of star formation, and, correspondingly relatively large populations of HMXBs. The X-ray luminosity registered at present for a given instantaneous SFR may then not correspond to the one obtained in galaxies for which strong interactions are not a prevailing characteristic, such as those used to obtain the L_X-SFR correlation.

Note that any excess in *early-type* CG galaxies cannot be explained as a metallicity effect. These systems are known to have high metallicities and estimated ages (Proctor et al. 2004; Mendes de Oliveira et al. 2005), even though the co-existence of old ellipticals with young spirals in some CGs suggests the possibility of replenishment with metal poor gas from the intergalactic medium (Diaferio et al. 1994). Early-type systems likely simply show large scatter which is a combination of local or background AGN contamination, hot gas, as well as stochastic effects.

7. CONCLUSIONS

This paper represents the first study of the contribution of individually detected X-ray point sources to the total X-ray luminosity, and its correlation with star formation rate and stellar mass, in a sample of 15 compact groups (47 galaxies). Our main results are:

1. The probability, $P_{\rm CG}$ that X-ray point sources detected within CG galaxy boundaries belong to the galaxy is high, with 87% of galaxies having $P_{\rm CG} \geq 0.8$.

2. Late-type galaxies:

   Excluding late-type galaxies that are known AGNs, have a single, nuclear X-ray point source, $L_X \geq 10^{41}$ erg s^{-1}, or have lower probability of hosting X-ray sources that are not background AGNs, 11 out of 12 galaxies (92%) have an X-ray luminosity which is higher than the one expected from the Mineo et al. (2012) L_X - SFR relation and its 1σ scatter. Excess luminosity appears to broadly correlate with the level of interaction/merging activity, with few exceptions.

3. Early-type galaxies:

   Excluding early-type galaxies that are known AGNs, have a single, nuclear X-ray point source, $L_X \geq$

10^{41} erg s^{-1}, or have lower probability of hosting X-ray sources that are not background AGNs, 8 out of 15 galaxies (53%) have an X-ray luminosity that shows a larger scatter than the Boroson et al. (2011) L_X - M_* relation.

4. Taking into account the luminosity detection limit for each galaxy, and the XRB XLFs of Mineo et al. (2012) and Gilfanov (2004) for late- and early-type galaxies, the probability of obtaining stochastically L_X values equal or higher to those observed is generally low, but increases for about half of the galaxies if there is strong XRB variability.

5. For non-AGN late-type galaxies the excess L_X per SFR in late-type systems is consistent with higher numbers of more luminous HMXBs or ULXs in low-metallicity environments, as observed in nearby low-metallicity galaxies and local Lyman Break Analogs.

6. The high L_X scatter for early-type systems likely has a variety of origins, including contamination from hot gas, background AGNs, local low-level AGN activity, as well as stochastic and variability effects.

Our results for late-type CG galaxies suggest that interactions can have a dramatic effect on star formation and XRB populations. However, not all interacting galaxies show excesses. This is likely related to the amount and location of the gas reservoir, or perhaps a more recent onset of interaction. Comparing XRB properties to the spatial distribution of star formation and gas content can further explore the nature of these effects.

A.H. and P.T. acknowledge funding provided through *Chandra* Award No. 15620513 issued by the *Chandra* X-Ray Observatory Center, which is operated by the Smithsonian Astrophysical Observatory under NASA contract NAS8-03060. We thank Andrew Ptak and Mihoko Yukita for useful discussions. We thank Bret Lehmer for making his catalog of star forming galaxies available to us. S.C.G., L.L. and T.D.D. thank the Natural Science and Engineering Research Council of Canada and the Ontario Early Researcher Award Program for support. This research has made use of data obtained from the High Energy Astrophysics Science Archive Research Center (HEASARC), provided by NASA's Goddard Space Flight Center. This research has made use of the NASA/IPAC Extragalactic Database (NED) which is operated by the Jet Propulsion Laboratory, California Institute of Technology, under contract with the National Aeronautics and Space Administration.

Facilities: Chandra, *Swift*, *Spitzer*

REFERENCES

Amram, P., Mendes de Oliveira, C., Plana, H., Balkowski, C., Hernandez, O., Carignan, C., Cypriano, E. S., Sodré, Jr., L., Gach, J. L., & Boulesteix, J. 2004, ApJ, 612, L5
Arnaud, K. A. 1996, in Astronomical Society of the Pacific Conference Series, Vol. 101, Astronomical Data Analysis Software and Systems V, ed. G. H. Jacoby & J. Barnes, 17
Barton, E., Geller, M., Ramella, M., Marzke, R. O., & da Costa, L. N. 1996, AJ, 112, 871
Basu-Zych, A. R., Lehmer, B. D., Hornschemeier, A. E., Gonçalves, T. S., Fragos, T., Heckman, T. M., Overzier, R. A., Ptak, A. F., & Schiminovich, D. 2013, ApJ, 774, 152
Bauer, F. E., Alexander, D. M., Brandt, W. N., Hornschemeier, A. E., Vignali, C., Garmire, G. P., & Schneider, D. P. 2002, AJ, 124, 2351
Bertin, E., & Arnouts, S. 1996, A&AS, 117, 393
Bitsakis, T., Charmandaris, V., Appleton, P. N., Díaz-Santos, T., Le Floc'h, E., da Cunha, E., Alatalo, K., & Cluver, M. 2014, A&A, 565, A25
Boroson, B., Kim, D.-W., & Fabbiano, G. 2011, ApJ, 729, 12
Broos, P. S., Townsley, L. K., Feigelson, E. D., Getman, K. V., Bauer, F. E., & Garmire, G. P. 2010, ApJ, 714, 1582
Cappelluti, N., Brusa, M., Hasinger, G., Comastri, A., Zamorani, G., Finoguenov, A., Gilli, R., Puccetti, S., Miyaji, T., Salvato, M., Vignali, C., Aldcroft, T., Böhringer, H., Brunner, H., Civano, F., Elvis, M., Fiore, F., Fruscione, A., Griffiths, R. E., Guzzo, L., Iovino, A., Koekemoer, A. M., Mainieri, V., Scoville, N. Z., Shopbell, P., Silverman, J., & Urry, C. M. 2009, A&A, 497, 635
de Vaucouleurs, G., de Vaucouleurs, A., Corwin, H. G., Buta, R. J., Paturel, G., & Fouque, P. 1991, Third Reference Catalogue of Bright Galaxies (Volume 1-3, XII, 2069 pp. 7 figs. Springer-Verlag Berlin Heidelberg New York)
Desjardins, T. D., Gallagher, S. C., Hornschemeier, A. E., Mulchaey, J. S., Walker, L. M., Brandt, W. N., Charlton, J. C., Johnson, K. E., & Tzanavaris, P. 2014, ApJ, 790, 132
Desjardins, T. D., Gallagher, S. C., Tzanavaris, P., Mulchaey, J. S., Brandt, W. N., Charlton, J. C., Garmire, G. P., Gronwall, C., Hornschemeier, A. E., Johnson, K. E., Konstantopoulos, I. S., & Zabludoff, A. I. 2013, ApJ, 763, 121
Diaferio, A., Geller, M. J., & Ramella, M. 1994, AJ, 107, 868
Douna, V. M., Pellizza, L. J., Mirabel, I. F., & Pedrosa, S. E. 2015, A&A, 579, A44
Durbala, A., del Olmo, A., Yun, M. S., Rosado, M., Sulentic, J. W., Plana, H., Iovino, A., Perea, J., Verdes-Montenegro, L., & Fuentes-Carrera, I. 2008, AJ, 135, 130
Eskew, M., Zaritsky, D., & Meidt, S. 2012, AJ, 143, 139
Fabbiano, G. 2006, ARA&A, 44, 323
Fabbiano, G., & Shapley, A. 2002, ApJ, 565, 908
Fedotov, K., Gallagher, S. C., Konstantopoulos, I. S., Chandar, R., Bastian, N., Charlton, J. C., Whitmore, B., & Trancho, G. 2011, AJ, 142, 42
Fixsen, D. J., Cheng, E. S., Gales, J. M., Mather, J. C., Shafer, R. A., & Wright, E. L. 1996, ApJ, 473, 576
Ford, G. P., Gear, W. K., Smith, M. W. L., Eales, S. A., Baes, M., Bendo, G. J., Boquien, M., Boselli, A., Cooray, A. R., De Looze, I., Fritz, J., Gentile, G., Gomez, H. L., Gordon, K. D., Kirk, J., Lebouteiller, V., O'Halloran, B., Spinoglio, L., Verstappen, J., & Wilson, C. D. 2013, ApJ, 769, 55
Fragos, T., Lehmer, B., Tremmel, M., Tzanavaris, P., Basu-Zych, A., Belczynski, K., Hornschemeier, A., Jenkins, L., Kalogera, V., Ptak, A., & Zezas, A. 2013, ApJ, 764, 41
Freeman, P. E., Kashyap, V., Rosner, R., & Lamb, D. Q. 2002, ApJS, 138, 185
Gallagher, S. C., Durrell, P. R., Elmegreen, D. M., Chandar, R., English, J., Charlton, J. C., Gronwall, C., Young, J., Tzanavaris, P., Johnson, K. E., Mendes de Oliveira, C., Whitmore, B., Hornschemeier, A. E., Maybhate, A., & Zabludoff, A. 2010, AJ, 139, 545
Gallagher, S. C., Richards, G. T., Hall, P. B., Brandt, W. N., Schneider, D. P., & Vanden Berk, D. E. 2005, AJ, 129, 567
Gehrels, N. 1986, ApJ, 303, 336
Gilfanov, M. 2004, MNRAS, 349, 146
Gilfanov, M., Grimm, H.-J., & Sunyaev, R. 2004a, MNRAS, 347, L57
—. 2004b, MNRAS, 351, 1365
Grimm, H.-J., Gilfanov, M., & Sunyaev, R. 2003, MNRAS, 339, 793
Hao, C.-N., Kennicutt, R. C., Johnson, B. D., Calzetti, D., Dale, D. A., & Moustakas, J. 2011, ApJ, 741, 124
Hickox, R. C., & Markevitch, M. 2006, ApJ, 645, 95
Hickson, P. 1982, ApJ, 259, 930
Hickson, P., Mendes de Oliveira, C., Huchra, J. P., & Palumbo, G. G. 1992, ApJ, 399, 353
Hopkins, P. F., & Quataert, E. 2010, MNRAS, 407, 1529

Hornschemeier, A. E., Heckman, T. M., Ptak, A. F., Tremonti, C. A., & Colbert, E. J. M. 2005, AJ, 129, 86
Jeltema, T. E., Binder, B., & Mulchaey, J. S. 2008, ApJ, 679, 1162
Johnson, K. E., Hibbard, J. E., Gallagher, S. C., Charlton, J. C., Hornschemeier, A. E., Jarrett, T. H., & Reines, A. E. 2007, AJ, 134, 1522
Kaaret, P., Schmitt, J., & Gorski, M. 2011, ApJ, 741, 10
Karachentsev, I. D. 2005, AJ, 129, 178
Kartaltepe, J. S., Sanders, D. B., Le Floc'h, E., Frayer, D. T., Aussel, H., Arnouts, S., Ilbert, O., Salvato, M., Scoville, N. Z., Surace, J., Yan, L., Capak, P., Caputi, K., Carollo, C. M., Cassata, P., Civano, F., Hasinger, G., Koekemoer, A. M., Le Fèvre, O., Lilly, S., Liu, C. T., McCracken, H. J., Schinnerer, E., Smolčić, V., Taniguchi, Y., Thompson, D. J., Trump, J., Baldassare, V. F., & Fiorenza, S. L. 2010, ApJ, 721, 98
Kennicutt, R. C. 1998, ARA&A, 36, 189
Kim, D.-W., Cameron, R. A., Drake, J. J., Evans, N. R., Freeman, P., Gaetz, T. J., Ghosh, H., Green, P. J., Harnden, Jr., F. R., Karovska, M., Kashyap, V., Maksym, P. W., Ratzlaff, P. W., Schlegel, E. M., Silverman, J. D., Tananbaum, H. D., Vikhlinin, A. A., Wilkes, B. J., & Grimes, J. P. 2004, ApJS, 150, 19
Kim, D.-W., Fabbiano, G., & Trinchieri, G. 1992, ApJ, 393, 134
Kirby, E. N., Cohen, J. G., Guhathakurta, P., Cheng, L., Bullock, J. S., & Gallazzi, A. 2013, ApJ, 779, 102
Konstantopoulos, I. S., Gallagher, S. C., Fedotov, K., Durrell, P. R., Heiderman, A., Elmegreen, D. M., Charlton, J. C., Hibbard, J. E., Tzanavaris, P., Chandar, R., Johnson, K. E., Maybhate, A., Zabludoff, A. E., Gronwall, C., Szathmary, D., Hornschemeier, A. E., English, J., Whitmore, B., Mendes de Oliveira, C., & Mulchaey, J. S. 2010, ApJ, 723, 197
Konstantopoulos, I. S., Gallagher, S. C., Fedotov, K., Durrell, P. R., Tzanavaris, P., Hill, A. R., Zabludoff, A. I., Maier, M. L., Elmegreen, D. M., Charlton, J. C., Johnson, K. E., Brandt, W. N., Walker, L. M., Eracleous, M., Maybhate, A., Gronwall, C., English, J., Hornschemeier, A. E., & Mulchaey, J. S. 2012, ApJ, 745, 30
Konstantopoulos, I. S., Maybhate, A., Charlton, J. C., Fedotov, K., Durrell, P. R., Mulchaey, J. S., English, J., Desjardins, T. D., Gallagher, S. C., Walker, L. M., Johnson, K. E., Tzanavaris, P., & Gronwall, C. 2013, ApJ, 770, 114
Kron, R. G. 1980, ApJS, 43, 305
Lee, B. C., Allam, S. S., Tucker, D. L., Annis, J., Johnston, D. E., Scranton, R., Acebo, Y., Bahcall, N. A., Bartelmann, M., Böhringer, H., Ellman, N., Grebel, E. K., Infante, L., Loveday, J., McKay, T. A., Prada, F., Schneider, D. P., Stoughton, C., Szalay, A. S., Vogeley, M. S., Voges, W., & Yanny, B. 2004, AJ, 127, 1811
Lehmer, B. D., Alexander, D. M., Bauer, F. E., Brandt, W. N., Goulding, A. D., Jenkins, L. P., Ptak, A., & Roberts, T. P. 2010, ApJ, 724, 559
Lehmer, B. D., Brandt, W. N., Alexander, D. M., Bell, E. F., Hornschemeier, A. E., McIntosh, D. H., Bauer, F. E., Gilli, R., Mainieri, V., Schneider, D. P., Silverman, J. D., Steffen, A. T., Tozzi, P., & Wolf, C. 2008, ApJ, 681, 1163
Leroy, A. K., Walter, F., Brinks, E., Bigiel, F., de Blok, W. J. G., Madore, B., & Thornley, M. D. 2008, AJ, 136, 2782
López-Sánchez, Á. R., Esteban, C., & Rodríguez, M. 2004, ApJS, 153, 243
Luo, B., Fabbiano, G., Fragos, T., Kim, D.-W., Belczynski, K., Brassington, N. J., Pellegrini, S., Tzanavaris, P., Wang, J., & Zezas, A. 2012, ApJ, 749, 130
Mamon, G. A. 1994, in Clusters of Galaxies, ed. F. Durret, A. Mazure, & J. Tran Thanh Van, 291
Mapelli, M., Colpi, M., & Zampieri, L. 2009, MNRAS, 395, L71
Mapelli, M., Ripamonti, E., Zampieri, L., Colpi, M., & Bressan, A. 2010, MNRAS, 408, 234
Mendes de Oliveira, C., Amram, P., Plana, H., & Balkowski, C. 2003, AJ, 126, 2635
Mendes de Oliveira, C., Coelho, P., González, J. J., & Barbuy, B. 2005, AJ, 130, 55
Mendes de Oliveira, C., Plana, H., Amram, P., Bolte, M., & Boulesteix, J. 1998, ApJ, 507, 691
Mihos, J. C., & Hernquist, L. 1996, ApJ, 464, 641
Mineo, S., Gilfanov, M., & Sunyaev, R. 2012, MNRAS, 419, 2095
Mukai, K. 1993, Legacy, vol. 3, p.21-31, 3, 21
Mulchaey, J. S. 2000, ARA&A, 38, 289
O'Sullivan, E., Vrtilek, J. M., David, L. P., Giacintucci, S., Zezas, A., Ponman, T. J., Mamon, G. A., Nulsen, P., & Raychaudhury, S. 2014a, ApJ, 793, 74
O'Sullivan, E., Zezas, A., Vrtilek, J. M., Giacintucci, S., Trevisan, M., David, L. P., Ponman, T. J., Mamon, G. A., & Raychaudhury, S. 2014b, ApJ, 793, 73
Persic, M., & Rephaeli, Y. 2007, A&A, 463, 481
Persic, M., Rephaeli, Y., Braito, V., Cappi, M., Della Ceca, R., Franceschini, A., & Gruber, D. E. 2004, A&A, 419, 849
Plana, H., Amram, P., Mendes de Oliveira, C., Balkowski, C., & Boulesteix, J. 2003, AJ, 125, 1736
Plana, H., Mendes de Oliveira, C., Amram, P., & Boulesteix, J. 1998, AJ, 116, 2123
Prestwich, A. H., Tsantaki, M., Zezas, A., Jackson, F., Roberts, T. P., Foltz, R., Linden, T., & Kalogera, V. 2013, ApJ, 769, 92
Proctor, R. N., Forbes, D. A., Hau, G. K. T., Beasley, M. A., De Silva, G. M., Contreras, R., & Terlevich, A. I. 2004, MNRAS, 349, 1381
Ranalli, P., Comastri, A., & Setti, G. 2003, A&A, 399, 39
Ribeiro, A. L. B., de Carvalho, R. R., Capelato, H. V., & Zepf, S. E. 1998, ApJ, 497, 72
Rieke, G. H., Alonso-Herrero, A., Weiner, B. J., Pérez-González, P. G., Blaylock, M., Donley, J. L., & Marcillac, D. 2009, ApJ, 692, 556
Rossa, J., van der Marel, R. P., Böker, T., Gerssen, J., Ho, L. C., Rix, H.-W., Shields, J. C., & Walcher, C.-J. 2006, AJ, 132, 1074
Saracco, P., & Ciliegi, P. 1995, A&A, 301, 348
Steffen, A. T., Brandt, W. N., Alexander, D. M., Gallagher, S. C., & Lehmer, B. D. 2007, ApJ, 667, L25
Surace, J. A., Sanders, D. B., Vacca, W. D., Veilleux, S., & Mazzarella, J. M. 1998, ApJ, 492, 116
Swartz, D. A., Soria, R., & Tennant, A. F. 2008, ApJ, 684, 282
Torres-Flores, S., Amram, P., Mendes de Oliveira, C., Plana, H., Balkowski, C., Marcelin, M., & Olave-Rojas, D. 2014, MNRAS, 442, 2188
Torres-Flores, S., Mendes de Oliveira, C., Amram, P., Plana, H., Epinat, B., Carignan, C., & Balkowski, C. 2010, A&A, 521, A59
Torres-Flores, S., Mendes de Oliveira, C., de Mello, D. F., Amram, P., Plana, H., Epinat, B., & Iglesias-Páramo, J. 2009, A&A, 507, 723
Tremmel, M., Fragos, T., Lehmer, B. D., Tzanavaris, P., Belczynski, K., Kalogera, V., Basu-Zych, A. R., Farr, W. M., Hornschemeier, A., Jenkins, L., Ptak, A., & Zezas, A. 2013, ApJ, 766, 19
Tremonti, C. A., Heckman, T. M., Kauffmann, G., Brinchmann, J., Charlot, S., White, S. D. M., Seibert, M., Peng, E. W., Schlegel, D. J., Uomoto, A., Fukugita, M., & Brinkmann, J. 2004, ApJ, 613, 898
Tzanavaris, P., Gallagher, S. C., Hornschemeier, A. E., Fedotov, K., Eracleous, M., Brandt, W. N., Desjardins, T. D., Charlton, J. C., & Gronwall, C. 2014, ApJS, 212, 9
Tzanavaris, P., Hornschemeier, A. E., Gallagher, S. C., Johnson, K. E., Gronwall, C., Immler, S., Reines, A. E., Hoversten, E., & Charlton, J. C. 2010, ApJ, 716, 556
Veilleux, S., Kim, D.-C., & Sanders, D. B. 2002, ApJS, 143, 315
Walker, L. M., Johnson, K. E., Gallagher, S. C., Charlton, J. C., Hornschemeier, A. E., & Hibbard, J. E. 2012, AJ, 143, 69
Walker, L. M., Johnson, K. E., Gallagher, S. C., Hibbard, J. E., Hornschemeier, A. E., Tzanavaris, P., Charlton, J. C., & Jarrett, T. H. 2010, AJ, 140, 1254
Werk, J. K., Putman, M. E., Meurer, G. R., Ryan-Weber, E. V., Kehrig, C., Thilker, D. A., Bland-Hawthorn, J., Drinkwater, M. J., Kennicutt, Jr., R. C., Wong, O. I., Freeman, K. C., Oey, M. S., Dopita, M. A., Doyle, M. T., Ferguson, H. C., Hanish, D. J., Heckman, T. M., Kilborn, V. A., Kim, J. H., Knezek, P. M., Koribalski, B., Meyer, M., Smith, R. C., & Zwaan, M. A. 2010, AJ, 139, 279
Xue, Y. Q., Luo, B., Brandt, W. N., Bauer, F. E., Lehmer, B. D., Broos, P. S., Schneider, D. P., Alexander, D. M., Brusa, M., Comastri, A., Fabian, A. C., Gilli, R., Hasinger, G., Hornschemeier, A. E., Koekemoer, A., Liu, T., Mainieri, V., Paolillo, M., Rafferty, D. A., Rosati, P., Shemmer, O., Silverman, J. D., Smail, I., Tozzi, P., & Vignali, C. 2011, ApJS, 195, 10
Zampieri, L., & Roberts, T. P. 2009, MNRAS, 400, 677